Magnetic Resonance Materials in Physics, Biology and Medicine (2025) 38:333–345
https://doi.org/10.1007/s10334-025-01237-3

RESEARCH ARTICLE

Fast whole brain relaxometry with Magnetic Resonance Spin TomograPhy in Time-domain (MR-STAT) at 3 T: a retrospective cohort study

Martin B. Schilder[1] · Stefano Mandija[1] · Sarah M. Jacobs[2] · Jordi P. D. Kleinloog[1] · Hanna Liu[1] · Oscar van der Heide[1] · Beyza Köktaş[1] · Federico D'Agata[3] · Vera C. W. Keil[4] · Evert-Jan P. A. Vonken[5] · Jan Willem Dankbaar[5] · Jeroen Hendrikse[5] · Tom J. Snijders[6] · Cornelis A. T. van den Berg[1] · Anja G. van der Kolk[5,7] · Alessandro Sbrizzi[1]

Received: 12 November 2024 / Revised: 4 February 2025 / Accepted: 7 February 2025 / Published online: 4 March 2025

Abstract

Objective To report T_1/T_2-values of normal and normal appearing brain tissues (NBTs, healthy volunteers; NABTs, patients) acquired with a whole-brain 5-minute Magnetic Resonance Spin TomograPhy in Time-domain (MR-STAT) protocol, and to explore relaxometry behavior in a brain tumor and in a multiple sclerosis patient.

Methods MR-STAT was acquired in 49 participants (39 patients with neurological pathologies, age range: 21–79 years) at 3 T. Mean T_1/T_2-values were computed for: normal and normal appearing grey matter (NGM/NAGM)/white matter (NWM/NAWM)/thalamus/putamen/caudate nucleus (CN)/globus pallidus (GP). Differences between sex, brain lobes, and left/right were assessed. The age-dependency of T_1/T_2-values in N(A)BTs was investigated. Relaxometry analysis was performed in two clinical case examples.

Results Mean (standard deviation) T_1/T_2-values were measured in N(A)GM = 1086(73)/74(9) ms; N(A)WM = 658(24)/48(3) ms; thalamus = 783(51)/42(4) ms; putamen = 863(40)/46(3) ms; CN = 1042(97)/63(9) ms; GP = 652(36)/36(3) ms. Differences between sex were not significant. T_1/T_2-values between the left/right parietal lobe and the left/right temporal lobe were significantly different. The quadratic age-dependency of T_1-values in the CN ($p = 0.00039$) and GP ($p = 0.00037$), and of T_2-values in the thalamus ($p = 0.00044$) and GP ($p = 0.003$) were significant. Pathological tissues could be discerned from NABTs using T_1/T_2-values.

Discussion T_1/T_2-values and data trends agree with literature, supporting the validity of MR-STAT as a clinical option for fast relaxometry despite the relatively low number of subjects in the study. Future work should aim to include healthy participants of a wider age-range and to include B_1-field corrections.

Keywords Magnetic resonance imaging · Relaxometry · Neuroimaging · Quantitative magnetic resonance imaging

Abbreviations

CN	Caudate nucleus
FLAIR	Fluid attenuated inversion recovery
GP	Globus pallidus
MR-STAT	Magnetic Resonance Spin TomograPhy in Time-domain

✉ Martin B. Schilder
m.b.schilder-2@umcutrecht.nl

[1] Computational Imaging Group for MR Therapy and Diagnostics, UMC Utrecht, Utrecht, Netherlands

[2] Department of Radiology and Nuclear Medicine, UMC Utrecht, Heidelberglaan 100, 3584 CX Utrecht, The Netherlands

[3] Department of Neurosciences, University of Turin, Turin, Italy

[4] Department of Radiology, Amsterdam UMC, Amsterdam, Netherlands

[5] Department of Radiotherapy, UMC Utrecht, Utrecht, Netherlands

[6] Department of Neurology & Neurosurgery, Brain Center, UMC Utrecht, Utrecht, Netherlands

[7] Department of Medical Imaging, Radboud UMC, Nijmegen, Netherlands

MRF	Magnetic Resonance Fingerprinting
MS	Multiple sclerosis
NABT	Normal appearing brain tissue
NAGM	Normal appearing grey matter
NAWM	Normal appearing white matter
NBT	Normal brain tissue
NGM	Normal grey matter
NWM	Normal white matter
PD	Proton density
PVE	Partial volume effect
QRAPTEST	Quantification of relaxation times and proton density by twin-echo saturation-recovery turbo-field echo
STAGE	STrategically Acquired Gradient Echo
syMRI	Synthetic magnetic resonance imaging
TrueFISP	True fast imaging with steady state precession

Introduction

Through magnetic resonance (MR) relaxometry, the magnetic properties T_1 and T_2 of human tissue can be measured [1]. Quantitative data potentially allows for unequivocal tissue characterization and might provide quantitative imaging biomarkers when compared to conventional, qualitative assessments. For instance, it has previously been shown that differences between Parkinson's disease patients and controls can be found based on relaxometry properties of cortical grey matter [2].

Over the past 20 years, brain relaxometry has undergone major developments. At the start of the twenty-first century, techniques like inversion recovery true fast imaging with steady state precession (TrueFISP) [3] and quantification of relaxation times and proton density by twin-echo saturation-recovery turbo-field echo (QRAPTEST) [4] were introduced. In more recent years, faster quantitative multiparametric magnetic resonance imaging (MRI) frameworks have been developed, such as MR Fingerprinting (MRF) [5–8], STrategically Acquired Gradient Echo (STAGE) [9–11], synthetic MRI (syMRI) [12, 13], MR Multitasking [14–16] and MR Spin TomogrAphy in Time-domain (MR-STAT) [1, 17, 18]. In this work, we focus on the latter technique.

MR-STAT is a multiparametric MRI technique that simultaneously maps T_1, T_2 and proton density (PD) from a 5-min acquisition [1, 18, 19]. The quantitative parameter maps are reconstructed by directly fitting a volumetric signal model to a transient-state time-domain signal. During the fitting, spatial localization of the signal and quantification of T_1, T_2 and PD are done simultaneously. The reconstruction is performed by numerically solving a large-scale non-linear problem. Recent advances in MR-STAT have included the clinical demonstration of synthetic MR-STAT images [20], accelerated parameter map reconstructions [21] and a 3D MR-STAT protocol for high-resolution knee imaging [22] and brain imaging [23]. Furthermore, good repeatability of MR-STAT has been demonstrated in gel phantoms [17, 24] and in vivo [23]. However, a study that reports relaxation times of normal brain tissues (NBT) in healthy volunteers and normal appearing brain tissues (NABTs) in patients of a cohort of relevant size using MR-STAT has not been presented.

The aim of this observational study is, therefore, to report T_1 and T_2 relaxation times of normal and normal appearing grey matter (NGM, in healthy volunteers/NAGM, in patients), normal and normal appearing white matter (NWM, in healthy volunteers/NAWM, in patients) and subcortical brain regions (thalamus, putamen, caudate nucleus and globus pallidus) measured at 3 T with MR-STAT in 49 subjects. In addition, we investigate: (a) differences in relaxation times between male and female participants to preliminarily assess bias towards sex; (b) differences between brain lobes to assess systematic biases; (c) left versus right differences within brain lobes to assess left–right biases; and (d) the relation between T_1- and T_2-values of N(A)BTs and age to find whether MR-STAT data confirms quadratic trends in T_1 and T_2 of N(A)GM, N(A)WM and subcortical brain regions that were described earlier in literature [25, 26]. If confirmed, values from NABTs could be used to preliminarily extend work on young healthy volunteers to elderly healthy volunteers. Lastly, our study concludes with two example cases of MR-STAT relaxometry in neurological brain disorders, namely a primary brain tumor and a multiple sclerosis (MS) lesion.

Methods

Study participants

Between October 2019 and October 2021, a total of 50 adult (≥ 18 years) subjects were included in the first MR-STAT clinical study [20]. The subjects were either healthy ($n = 10$), defined as lacking history of neurological disease and no imaging findings to suspect otherwise, or had the clinical diagnosis of primary brain tumor ($n = 11$), ischemic stroke ($n = 10$), epilepsy ($n = 10$) or MS ($n = 9$). The study was registered in the international clinical trials registry platform with number NL8437 (https://trialsearch.who.int/Trial2.aspx?TrialID=NL-OMON26690) and was conducted according to the guidelines described in the Declaration of Helsinki, and approved by the Institutional Review Board (NL69544.041.19, METC 19/282). Written informed consent was given by all participants prior to scanning. Example images of the quantitative parameter maps (T_1, T_2, PD) and conventional and synthetic contrast weighted images

including all 30 slices from a healthy participant and a patient of each group are in a publicly available repository (https://gitlab.com/asbrizzi/mr-stat-synthetic-images).

For the current study, all patients were retrospectively included in this analysis from the above-mentioned trial. However, one patient had a large bilateral stroke and NABTs could thus insufficiently be identified. This patient was retrospectively excluded from our analysis since the primary focus of this study is to report on relaxation times of N(A)BTs. In addition, if an epilepsy patient had a (benign) tumor as underlying cause of the symptoms, this patient was transferred to the tumor group, which was the case for six epilepsy patients. This led to a study population consisting of 10 healthy volunteers, 17 tumor patients, 9 stroke patients, 4 epilepsy patients and 9 MS patients. A summary of the study population can be found in Table 1.

Acquisition and processing

MRI acquisitions were performed on an Ingenia scanner (Philips Healthcare, Best, the Netherlands) at 3 T using a clinical 15 channel receiver head coil (Philips Healthcare, Best, the Netherlands). Conventional contrast weighted scans (T_1w, T_2w, PDw, FLAIR) and MR-STAT were acquired. The exact sequence parameters are listed in Table 2. The MR-STAT sequence consisted of multiple Cartesian-encoded 2D slices. Each slice was sequentially acquired with a gradient-spoiled gradient echo scheme and a slowly varying flip angle with amplitude between 0° and 90°. The flip angle train is shown in Supplementary Material A. Each RF train was preceded by a non-selective inversion pulse [17]. In total, 30 axial slices with $1 \times 1 \times 3$ mm^3 resolution and an interslice gap of 1.5 mm were acquired. Scan time for the MR-STAT protocol was roughly 5 min. The reconstruction was performed according to methods presented in Liu et al., consisting of an alternating direction method of multipliers [21]. The offline reconstruction time was approximately 2 min per slice.

Synthetic T_1w images were generated using an analytical signal model as described in more detail in Kleinloog et al. [20]. Automatic brain tissue segmentations were performed on the synthetic T_1w images using the software Vol2brain [27] for the following cerebral brain structures: cortical grey matter, cortical white matter, thalamus, putamen, caudate nucleus, and globus pallidus. Due to the limited spatial resolution in the craniocaudal direction, the cerebellum was excluded from the analysis. Vol2brain also provided masks for each brain lobe and a hemisphere mask. For all patients, lesions were manually segmented using FSL software [28] and were subtracted from all other masks. This lead to masks for NABTs, that we defined as patients' tissues without visible lesions.

Table 1 Summary of patient population

Group	*N*	Male/female	Mean age in years (standard deviation)
Total population	49	27/22	44.2 (16.1)
Healthy volunteers	10	6/4	24.2 (2.7)
Tumor patients	17	10/7	47.9 (14.5)
Stroke patients	9	4/5	51.8 (14.5)
Epilepsy patients	4	3/1	50.8 (15.0)
Multiple sclerosis patients	9	4/5	45.9 (12.9)

Preliminary test: relaxation times of NBTs and NABTs

Twelve out of seventeen tumor patients had received radiotherapy prior to this study. To test if the T_1- and T_2-values of NAGM and NAWM differed significantly between the tumor patient group that did receive radiotherapy and the

Table 2 Acquisition parameters of MR-STAT imaging and conventional imaging. An axial scan orientation was used

Imaging parameters	MR-STAT Spoiled GRE	T_1w SE	T_2w SE	PDw TSE	FLAIR TSE
FOV	$224 \times 224 \times 133.5$ mm^3				
Spatial resolution	$1 \times 1 \times 3$ mm^3				
Gap	1.5 mm				
Slices	30				
TR (ms)	8.9	451	3400	2800	10,000
TI (ms)	–	–	–	–	2800
TE (ms)	4.7	14	80	20	120
Flip angle	Variable	70	90	90	90
TSE factor	–	–	15	14	24
Scan time	5:11 min	3:16 min	1:44 min	3:40 min	1:41 min

MR-STAT: Magnetic Resonance Spin TomogrAphy in Time-domain; *PD:* Proton Density weighted; *FLAIR:* Fluid Attenuated Inversion Recovery; *GRE:* gradient echo; *SE*: spin echo; *TSE:* turbo spin echo; *FOV:* field of view; *TR:* repetition time; *TI:* inversion time; *TE:* echo time

tumor patient group that did not, a Mann–Whitney U test was performed with a significance level of 0.05. Bonferroni correction was not performed to prevent making type II errors. Next, the mean T_1- and T_2-values were computed for the N(A)GM, N(A)WM and for the normal and normal appearing thalamus, putamen, caudate nucleus and globus pallidus. These values were reported for both the healthy participants and the complete study population.

Statistical analysis

All statistical tests were performed in MATLAB 2019A (MathWorks, Natick, MA, USA). For the sex-related differences and comparison between brain lobes (tests 1–3), only data from healthy volunteers was used. However, to perform meaningful statistical tests with respect to dependency of T_1- and T_2-values on age (test 4), a wider age-interval was needed. Therefore, data from NBTs from healthy volunteers and data from NABTs from patients were bundled in this part of the analysis. For each of the tests, a significance level of 0.05 was used before Bonferroni correction was applied. The corresponding significance level is mentioned for each of the tests.

Test 1: Sex-related differences

A Mann–Whitney U test was used to test if there were sex-related differences within the study population between the T_1-values and T_2-values of NGM and NWM. Since this test included a small sample (male participants: $n = 6$; female participants: $n = 4$), no meaningful assumption about the underlying distribution (e.g. a normal distribution) could be made. Therefore, a non-parametrical test with Bonferroni correction was applied. The corresponding significance level was 0.0125. To ensure age was not a confounding factor, another Mann–Whitney U test was performed to test if there were significant differences in age between the male and female group.

Test 2: Differences between brain lobes

The T_1-values of NGM and NWM from the frontal, parietal, occipital and temporal brain lobes were compared. Here, data from both the left and right hemispheres were bundled. A Wilcoxon signed rank with Bonferroni correction and a corresponding significance level of 0.0021 was used. As B_1-effects confound the T_2-values, we did not test for significance in T_2-values.

Test 3: Left–right brain lobe differences

In this test, T_1- and T_2-values of NGM and NWM of the left versus right brain lobes were compared to test whether differences were statistically significant. For this comparison, a Wilcoxon signed rank test with Bonferroni correction and a corresponding significance level of 0.0031 was used.

Test 4: Dependency of relaxation times on age

A quadratic curve was fit to T_1- and T_2-values of N(A)GM, N(A)WM and normal (appearing) thalamus, putamen, caudate nucleus and globus pallidus. The function that was fit was $T(\text{age}) = a \times \text{age}^2 + b \times \text{age} + c$. The use of a quadratic curve to fit T_1 and T_2 of N(A)GM, N(A)WM and subcortical brain regions was described earlier in literature [25, 26]. An F-test with Bonferroni correction was performed to determine if a quadratic function fitted the data better than a linear function, with a corresponding significance level of 0.0042.

Case examples

To further demonstrate the potential of quantitative MRI using MR-STAT, this paper was concluded with two case examples, namely for a tumor patient and an MS patient. A case example for a stroke patient was not provided since the stroke events for the included patients occurred several months or even years prior to data acquisition. Regarding the epilepsy group, since the causes of the epilepsy were either no longer visible (because of previous surgery), or consisted of sclerosis of the hippocampus (which was not part of this analysis), no example case from the epilepsy group was provided.

Case example 1: Tumor patient

The first example case describes the T_1- and T_2-findings of a tumor patient. The imaging findings from this patient were selected because no treatment had been given at the time of scanning (and thus the quantitative values had not been influenced by treatment effects), and because the lesion was well delineable. The NAGM, NAWM and lesions were segmented according to methods described above. As a contrast agent was not administered, the enhancement status of the tumor is unknown.

Case example 2: Multiple sclerosis patient

The second case report concerns a patient with MS. The NAGM, NAWM and lesions were segmented according to methods described above. An analysis of T_1- and T_2-values was performed on one lesion that clearly shows as a T_1 black hole. Since no contrast agent was administered, the enhancement status of the lesion is unknown.

Results

Preliminary test: relaxation times of NBTs and NABTs

No statistically significant differences were found between T_1 of NAGM and NAWM and T_2 of NAGM and NAWM of tumor patients that had undergone radiotherapy treatment prior to this study, versus tumor patients that had not ($p = 0.6787$, $p = 0.9530$, $p = 0.6787$, $p = 0.8591$, respectively). However, because the group had been treated with radiotherapy, the groups remained split for further analysis.

The mean T_1- and T_2-values over the segmented brain regions are reported in Table 3 for the healthy participants and for the population as a whole. A further breakdown per patient group was provided in Supplementary Material B.

Statistical analysis

Test 1: Sex-related differences

Differences in age between the group were not statistically significant ($p = 0.8762$). Age was thus comparable between the groups. Figure 1 shows boxplots of T_1 and T_2 of NGM and NWM of the male and female healthy participants. No statistically significant differences were found between the T_1 and T_2 of NGM and NWM of male and female subjects ($p = 0.580$, $p = 0.330$, $p = 0.944$, $p = 0.350$).

Table 3 Mean and standard deviations of T_1 and T_2 of NBTs from healthy volunteers and N(A)BTs from the mixed clinical population and literature

Brain region	Mean T_1 (±SD) [ms]			Mean T_2 (±SD) [ms]		
	Healthy volunteers ($n = 10$)	Total population ($n = 49$)	Literature ranges [7, 8, 11, 13, 14, 25, 26, 29–45]	Healthy volunteers ($n = 10$)	Total population ($n = 49$)	Literature ranges [7, 8, 11, 13, 14, 25, 26, 29–45]
N(A)GM	1136 (82)	1086 (73)	790–1618	77 (12)	74 (9)	53–130
N(A)WM	657 (18)	658 (24)	620–954	48 (3)	49 (3)	29–120
Thalamus	771 (49)	783 (51)	860–1262[a]	40 (3)	42 (4)	60–74[a]
Putamen	878 (47)	863 (40)	920–1328[a]	46 (4)	46 (3)	49–64[a]
Caudate nucleus	1028 (69)	1042 (97)	960–1379[a]	61 (8)	63 (9)	59–73[a]
Globus pallidus	664 (24)	652 (36)	800–1055[a]	36 (2)	36 (3)	–

[a] Mean T_1- or T_2-values were not always explicitly provided in early published literature. Thus, values from individual study participants were estimated from the figures in the publication

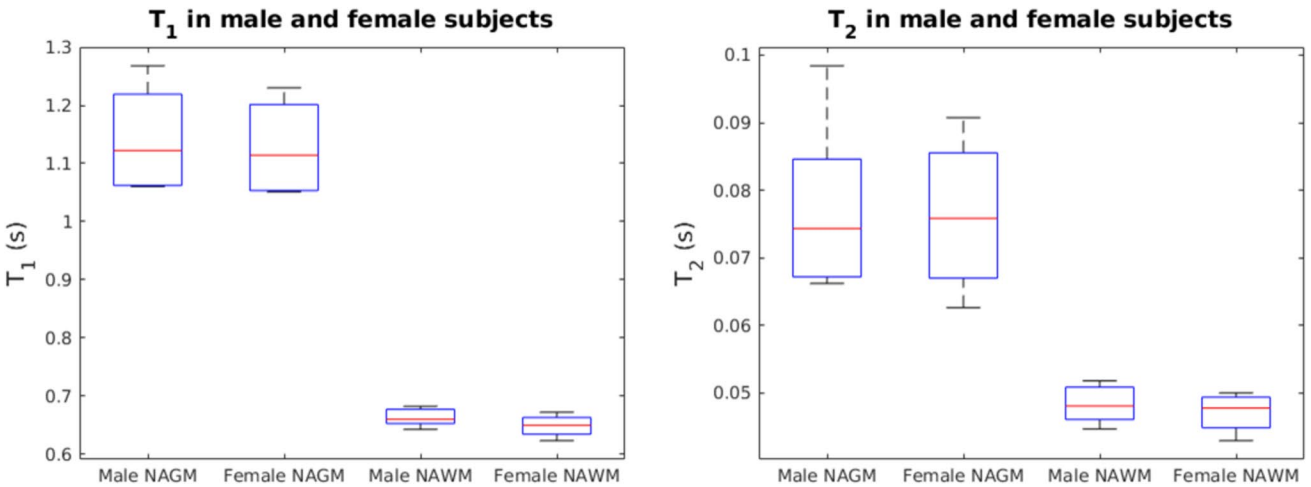

Fig. 1 Boxplots comparing T_1- and T_2-values of NGM and NWM between male and female subjects. The mean age of the male population was 24 (±1.8) years. The mean age of the female population was 24.5 (±4.0) years. Differences in age between the group were not statistically significant ($p = 0.8762$). Age was thus comparable between the groups. The red line indicated the median, the box indicates the upper quartile and the lower quartile and the whiskers indicate one standard deviation above and below the mean

Test 2: Differences between brain lobes

Figure 2 shows the boxplots of T_1 and T_2 of NGM and NWM for each brain lobe. In the comparison between brain lobes, for the T_1 of NGM and NWM, no significant differences between brain lobes were found. A table with p-values for all comparisons can be found in Supplementary Material C.

Test 3: Left–right brain lobe differences

Statistically significant differences were found between the T_1 of NGM of the left versus the right temporal lobe, between the T_1 of NGM of the left versus right parietal lobe, between the T_1 of NWM of the left versus right parietal lobe and between the T_2 of NWM of the left versus right temporal lobe. All other differences were not significant. Statistically significant differences between hemispheres were thus limited to the parietal lobe and in the temporal lobe. A table with p-values was provided in Supplementary Material D.

A table with T_1- and T_2-values per brain lobe was provided in Supplementary Material E.

Test 4: Dependency of relaxation times on age

In Fig. 3, the quadratic fits for age and T_1 and T_2 of N(A)GM and N(A)WM are shown. For the T_1 of N(A)GM, the coefficient of determination resulted to be $R^2 = 0.124$ ($p = 0.048$) and for the T_1 of N(A)WM, $R^2 = 0.196$ ($p = 0.007$). We found $R^2 = 0.136$ ($p = 0.035$) for the T_2 of N(A)GM and $R^2 = 0.146$ ($p = 0.027$) for the T_2 of N(A)WM. The minima of the four curves were found at 50 years, 35 years, 48 years and 41 years, respectively. The quadratic fits for the T_1 of the caudate nucleus ($p < 0.001$) and the globus pallidus ($p < 0.001$) and the T_2 of the thalamus ($p < 0.001$) and the

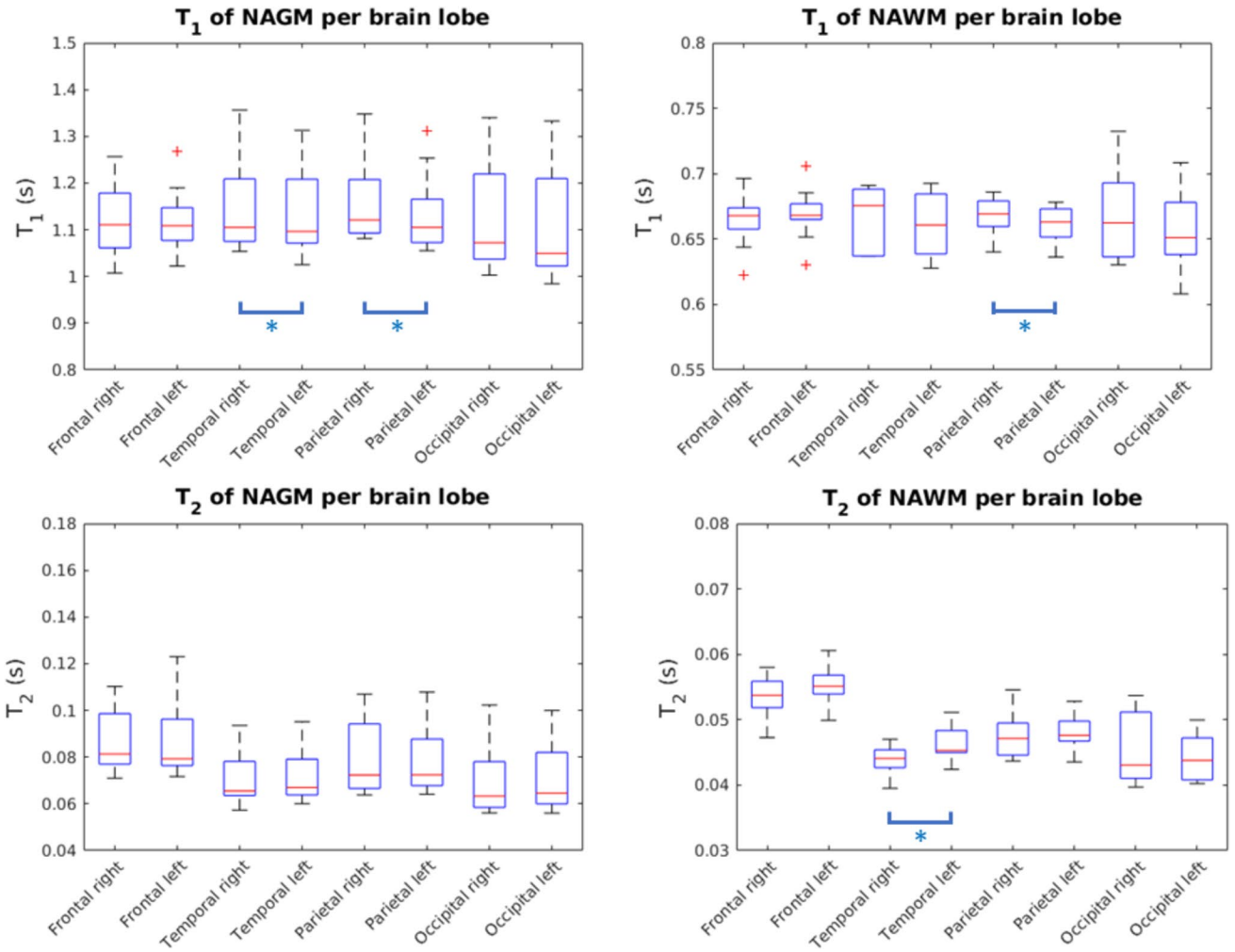

Fig. 2 Boxplots visualizing T_1- and T_2-values of NGM and NWM per brain lobe. Only data from healthy volunteers was used. There were no significant results from test 2. Blue bars: single asterisks indicates significant differences between lobes from the left versus right hemisphere. All other differences were not significant (test 3)

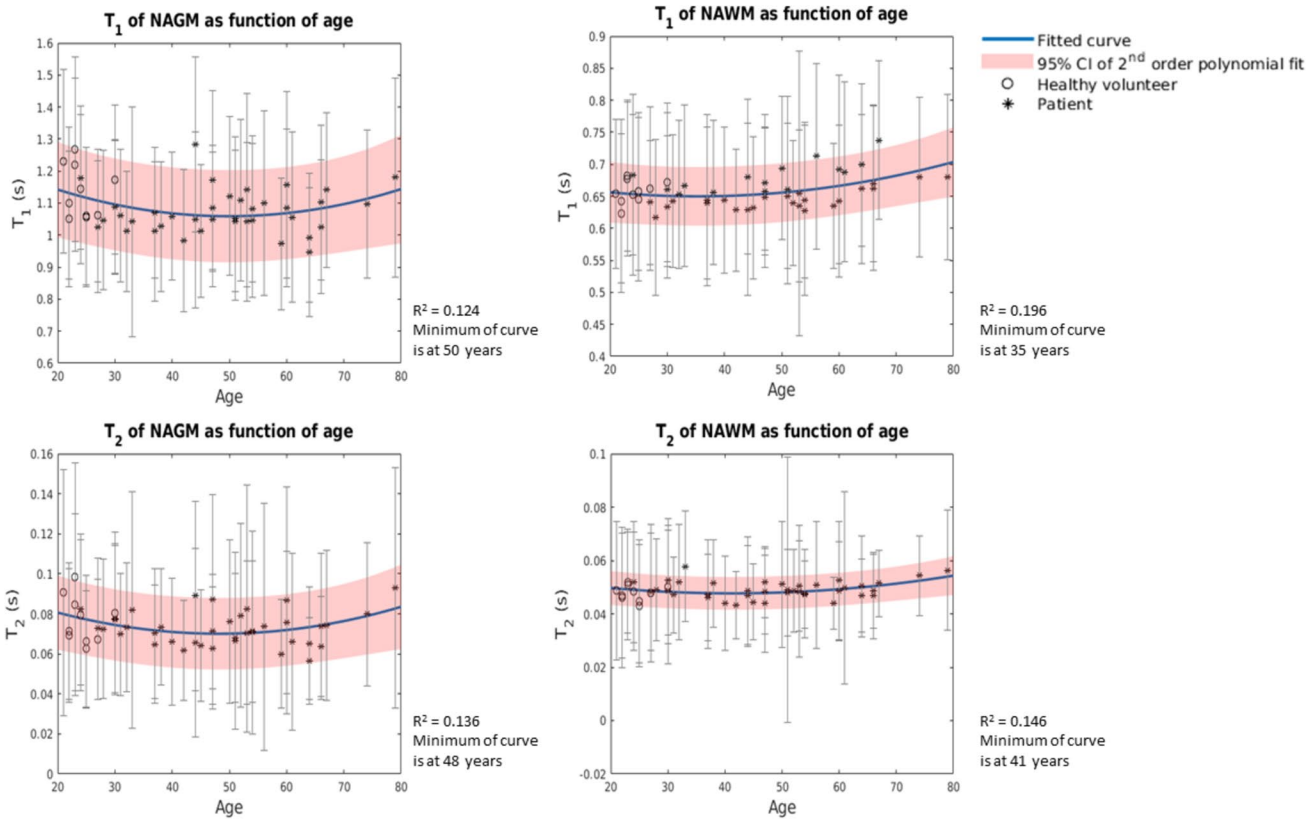

Fig. 3 Fitted quadratic curves for T_1 and T_2 of N(A)GM and N(A)WM. The blue curve indicates the fitted model. The red lines indicate the 95% confidence interval of the fit. The bars in the plot through the datapoints indicate the standard deviation of T_1 and T_2 within N(A)GM and N(A)WM

globus pallidus ($p = 0.003$) were significant. All other quadratic fits were not statistically significant. An overview of the exact coefficients of determination, p-values and the coefficients of the quadratic fit for the N(A)BTs can be found in Supplementary Material F. Overall, we observed a quadratic trend, which is in line with earlier literature [6, 25, 26].

Case examples

Case example 1: Anaplastic glioma

Figure 4 shows the conventional T_1w image, the conventional FLAIR, the T_1-map, the T_2-map and a scatterplot with histograms visualizing the quantitative data distribution for the tumor patient with an anaplastic glioma (WHO 2021 diagnosis: Diffuse glioma grade 3, not elsewhere classifiable). For this patient, the mean T_1 (SD) of the anaplastic glioma (red arrow) was 1729 (353) ms and the mean T_2 (SD) was 140 (53) ms. For the NAGM, the mean T_1- and T_2-values (SD) were 992 (202) ms and 65 (28) ms, respectively, while for the NAWM, the mean T_1- and T_2-values were 661 (116) ms and 50 (19) ms, respectively. The lesion's T_1 showed an increase of 74.3% and 161.4% compared to NAGM and NAWM, while the lesion's T_2 showed an increase of 114.4% and 177.8% compared to NAGM and NAWM.

Case example 2: Multiple sclerosis

In the second case, a patient with MS was investigated. Figure 5 shows the corresponding anatomical images (conventional T_1w, conventional FLAIR), as well as quantitative maps (T_1, T_2) and a scatterplot with histograms visualizing the quantitative data distributions for each tissue of interest. One of the MS lesions has been denoted with a red arrow. For the selected lesion, the mean T_1 (SD) was 1084 (408) ms and the mean T_2 (SD) was 87 (48) ms. Of the NAWM, the mean T_1 was 643 (104) ms and the mean T_2 was 47 (14) ms. This means that the lesion's T_1 showed an increase of 68.6%, while the lesion's T_2 showed an increase of 85.1% compared to the T_1 and T_2 of NAWM.

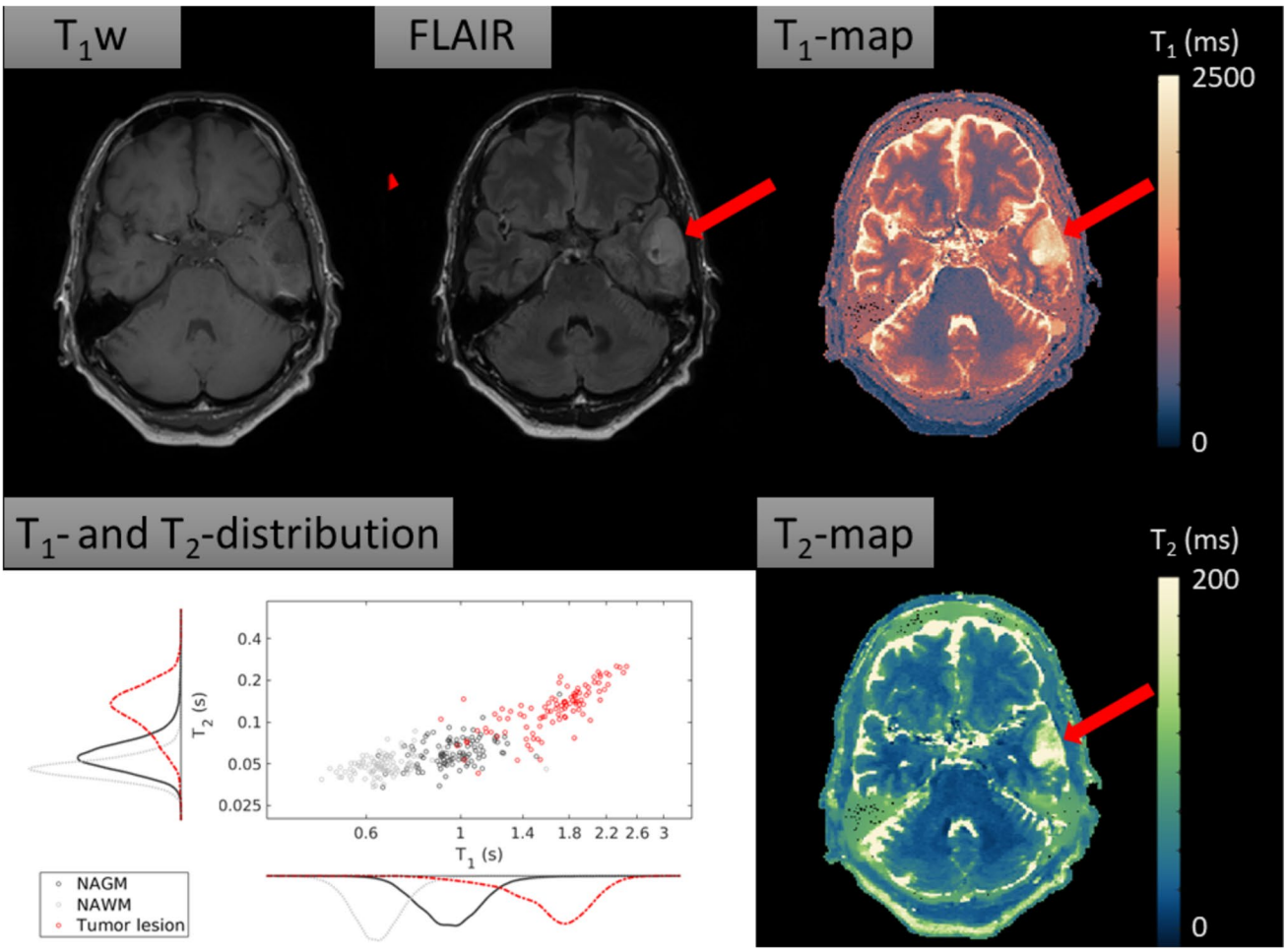

Fig. 4 The conventional T_1w image shows an intra-axial hypointense tumor. The conventional FLAIR image shows a hyperintense tumor. The red arrow denotes the tumor. The T_1-map and the T_2-map show elongation of T_1- and T_2-values in the tumor compared to the surrounding NABTs. Scatterplot and histogram of marginal T_1 and T_2 distributions for each tissue of interest. The quantitative data distribution for the T_1-values and for the T_2-values of the tumor are mostly separable from the NAGM and NAWM. The scatterplot was randomly under-sampled for legibility

Discussion

Summary of main findings

In order to add to the validity of MR-STAT as a clinically applicable fast relaxometry technique, this study sought to report T_1- and T_2-values of NBTs and NABTs acquired in 49 participants. Differences between male and female participants were not statistically significant. Furthermore, statistically significant differences in relaxation times across hemispheres were seen in the parietal lobe and in the temporal lobe. We found a significant quadratic age-dependency of T_1 of the caudate nucleus, T_1 of the globus pallidus, T_2 of the thalamus and T_2 of the globus pallidus. All other quadratic age-dependencies were not statistically significant. Lastly, in two individual case examples, quantitative values of pathological tissues were presented, i.e. for a tumor patient and an MS patient, with clear differences between lesions versus normal tissues.

Comparison to literature

The relaxation times of N(A)GM and N(A)WM reported in this paper are within ranges of relaxation times at a field strength of 3 T reported in recent literature (T_1: NAGM = 790–1618 ms; NAWM = 620–954 ms; T_2: NAGM = 53–130 ms; NAWM = 29–120 ms) [7, 8, 11, 13, 14, 25, 26, 29–45]. The measured T_1- and T_2-values of thalamus, putamen, caudate nucleus and globus pallidus were lower than or at the lower end of earlier reported ranges (T_1: thalamus = 860–1262 ms; putamen = 920–1328 ms; caudate nucleus = 960–1379 ms; globus pallidus = 800–1055 ms; T_2: thalamus = 60–74 ms; putamen = 49–64 ms; caudate

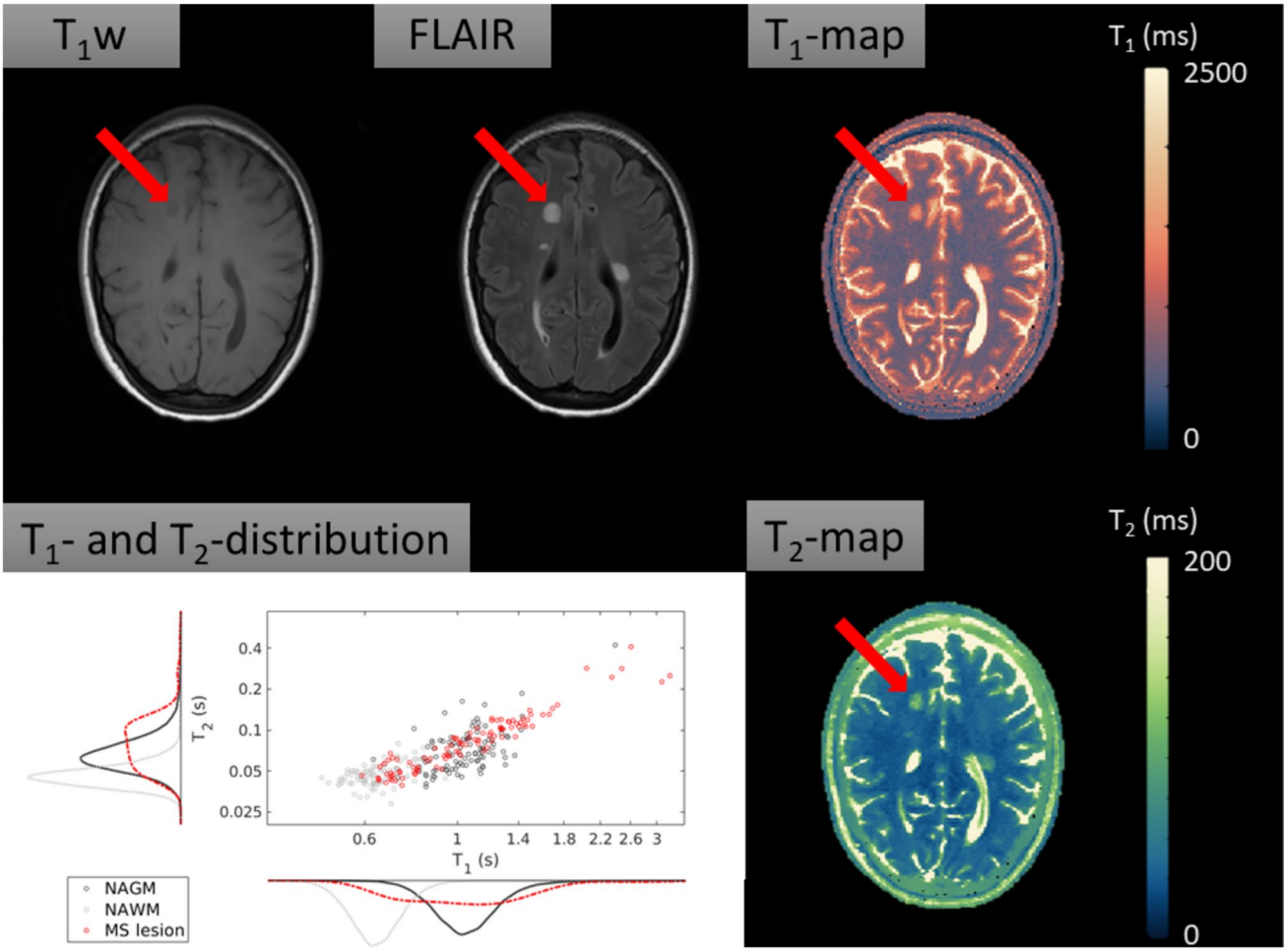

Fig. 5 Conventional anatomical images (T_1w, FLAIR), quantitative maps (T_1, T_2) and a scatterplot with histograms visualizing the quantitative data distributions for each tissue of interest. T_1w image shows multiple hypointense black-hole lesions, which are typical for MS. FLAIR image shows multiple corresponding hyperintense lesions. The T_1-map shows that the lesions have on average longer T_1 values than the normal appearing surrounding tissue. The T_2-map shows longer a transverse relaxation time of the lesion compared to surrounding NAWM. The scatterplot with quantitative data distribution shows that, compared to the NAWM, the lesion does no longer have similar T_1- and T_2-values The scatterplot was randomly undersampled for legibility

nucleus = 59–73 ms; globus pallidus = not available) [7, 8, 11, 13, 14, 25, 26, 29–45].

Earlier work using MR-STAT relaxometry in gel phantoms presented good correlation with ground truth values [17, 46]. However, in vivo, confounding factors that potentially influence the measured T_1- and T_2-values include the magnetization transfer (MT) effect, subject motion and flow of blood and cerebrospinal fluids. MT effects are not described in the Bloch equations that are used in the MR-STAT framework. However, it was demonstrated in MRF-based experiments that correcting for MT leads to an increase of 12–25% for T_1, and 16–34% for T_2, where the effects of MT corrections was generally stronger in more myelinated tissues [45]. Possibly, not correcting for MT contributed also to the relatively low reported T_1- and T_2-values observed in our study. No motion artefacts were observed and flow related artefacts were confined to the ventricles according to radiological assessment [20]. Consequently, the effect of motion and flow on the presented T_1- and T_2-values of NBTs, NABTs and lesions is likely negligible.

Regarding the differences in relaxation times of NGM and NWM between male and female participants, no statistically significant differences were found. Earlier literature also reported that no statistically significant differences were found [8, 26]. With respect to the left–right brain lobe comparison, we found statistically significant left–right differences in the T_1 of NGM of the temporal lobe, in the T_2 of the NWM of the parietal lobe and the temporal lobe, and in the T_2 of the NWM of the temporal lobe. Earlier literature describes hemispheric asymmetries for the T_1 of NWM of the temporal lobe, the T_2 of NWM of the frontal lobe and the T_2 of NWM of the parietal lobe [6]. The statistically

significant differences we found could be attributable to microstructural differences that originate from unilateral dominance for language, lateralization of spatial recognition and WM connectivity [47]. Concerning the differences between brain lobes, the differences were not statistically significant for the T_1 of NGM and NWM.

Age-dependencies of T_1- and T_2-values of the N(A)GM, N(A)WM, thalamus, putamen, caudate nucleus and globus pallidus were investigated. Using an established quadratic model [26], we found that the age-dependencies for T_1-values of the caudate nucleus and the globus pallidus, and the T_2-values of the thalamus and the globus pallidus were statistically significant. Similar results were found in literature for the age-dependency of T_1-values of the caudate nucleus [26], T_1-values of the globus pallidus [25] and the T_2-values of the thalamus [26]. However, the relationship between age and T_2-values for the globus pallidus was not addressed in recent literature. Although the quadratic relationships were not significant for all brain regions, a quadratic trend was observed in our data, similar to earlier literature [6, 25, 26]. Factors that contribute to these quadratic models for relaxation times include non-pathological age-related loss of myelination, increased free water content and ion depositions [6, 25, 26]. However, in the current analysis, the potential influence of disease progression on relaxation times of NABTs cannot be excluded and literature on this topic is scarce. Also, there is no consensus in literature on whether to use a linear fit, a quadratic fit or a more complex fit to model age-dependencies of relaxation times of brain regions, nor is there consensus on whether this differs per brain region. However, the strong relationship between age and relaxation times underlines the importance of age when considering normative T_1- and T_2-values for N(A)BTs.

With respect to the case examples, we reported a mean T_1 of 1729 ($\pm$353) ms and a mean T_2 of 140 ($\pm$53) ms for the grade 3 anaplastic glioma. Springer et al. reported average T_1-values ranging between 1770 and 2068 ms, and average T_2-values ranging between 79 and 144 ms for grade 3 glioma [48], which fall within one standard deviation from our measurements. Regarding the multiple sclerosis case study, the lesion in our patient showed an increase of 68.6% in T_1-values and increase of 85.1% in T_2-values when compared to the quantitative values of NAWM. The increased T_1- and T_2-values can be explained by the inflammatory and demyelinating brain pathology in MS patients [49]. At 1.5 T [50], the reported T_1-values of enhancing and non-enhancing lesions were on average 40.2% and 92.1% higher than the average T_1-values of NAWM. Reported T_2-values of enhancing and non-enhancing lesions were on average 33.7% and 77.0% higher than the T_2-values of NAWM for the study population as a whole. A direct comparison of relaxation times was not possible, since the studies were performed at different field strengths and the enhancement status of our patient's lesion is unknown. Yet, the percentage wise increase confirms characteristics of MS lesions described in earlier literature. Overall, in diseased tissues, similar trends were observed in T_1- and T_2-values measured with MR-STAT and T_1- and T_2-values reported in literature. This offers preliminary support for the clinical validity of MR-STAT as fast relaxometry protocol.

Limitations

Firstly, statistical tests 1–3 necessitate cautious interpretation. Only data from young, healthy participants was used, and the results might therefore lack generalizability for an elderly population. Moreover, we compared male healthy volunteers ($n=6$) against female healthy volunteers ($n=4$) in test 1. Due to relatively low number, the robustness of this test is limited. We believe the validity of tests 2 and 3 ($n=10$) remains reasonably strong, indicating there is no systematic left/right bias and thus preliminarily supporting the clinical utility of MR-STAT.

Secondly, our study population is heterogeneous in terms of age, sex and clinical status. Also, despite our efforts to exclude all pathological tissue from the statistical tests, it is still possible that some of this tissue was erroneously classified as NABTs. In particular, we are aware that MS patients can have elevated T_2-values (approximately 2 ms higher) in the parietal and temporal NAWM [51]. However, in the current study, patient data from NABTs were used in the age-dependency analysis only and the trends observed in this analysis aligned with literature.

Thirdly, due to the spatial resolution of the current sequence, data might be subject to partial volume effects (PVE) or relevant tissues might be partially missing. We observed that we measured T_1- and T_2-values in subcortical brain regions that were lower than or at the lower end of values in literature. Potentially, the mean relaxation times of the subcortical brain regions have been offset by surrounding NAWM that might have contaminated the corresponding masks. Furthermore, the PVE might be reflected in the span of T_1- and T_2-values in the N(A)GM, which are globally wider than the T_1- and T_2-values of N(A)WM as an effect of CSF contamination of the N(A)GM mask (Fig. 2). Locally, a relatively wide span in T_1-values of N(A)GM of the occipital lobe is observed compared to the other brain lobes. As the N(A)GM of the occipital lobe is thinner compared to the N(A)GM of the other brain lobes [52], more PVE might occur. An example of a relevant missing subcortical nucleus is the substantia nigra, which is an important region to image in the diagnosis of Parkinson's disease [53]. To alleviate PVE and to ensure no relevant tissues are missing, future work should focus on creating a 2D MR-STAT sequence with isotropic resolution without interslice gaps, or on creating a 3D MR-STAT sequence [22, 23].

Lastly, since we compared multiple variables in each statistical test, we performed Bonferroni correction extensively. This reduces the chance of finding statistically significant differences, however, at the cost of increased chance of making type I errors. Some findings may thus incorrectly have been regarded as not statistically significant.

Clinical relevance

The reported relaxometry values could be used as reference values for NBTs and NABTs in future research that uses this sequence. In the case examples we provided, diseased tissue could clearly be discerned from NABTs using quantitative values. This opens up possibilities for voxel based clustering and other automated classification and segmentation methods in the future. We would like to stress that more research with clearly defined, sufficiently sized cohorts is needed to prove the value of MR-STAT in addition to or as substitute of conventional MRI.

Future outlook

Whereas the current work focused on NBTs and NABTs, future work involving MR-STAT should shift its attention to finding added value to clinical routine. One possible direction is to leverage the values from the quantitative parameter maps for data science and machine learning purposes, such as tumor classification or anomaly detection. One publication describes the use of MRF to differentiate between two subtypes of glioma by analyzing the quantitative values of the solid parts of the tumors, the peritumoral edema and the NAWM [48]. In another study, methods to build voxel-wise quantitative brain relaxation atlases are described. The quantitative relaxation atlases are then used to compute a voxel-wise statistical deviation map. Using these deviation maps, MS lesions could clearly be identified from NABTs [54]. Potentially, these applications could help guide clinicians in their decision-making with the support of automated data-analysis tools.

Conclusion

In this study, relaxation times and data trends of NBTs and NABTs using MR-STAT data of 49 subjects were reported for the first time. Furthermore, two individual clinical cases were presented using MR-STAT in a clinical context. Since our findings were generally in line with earlier relaxometry literature, this work preliminarily adds to the validity of MR-STAT as a clinically feasible option for fast relaxometry. More research is needed to define, improve and validate its clinical value.

Supplementary Information The online version contains supplementary material available at https://doi.org/10.1007/s10334-025-01237-3.

Acknowledgements We would like to thank Carlo Lucci from the University Medical Center Utrecht for supporting with the data acquisition process. Also, we express our gratitude to Shanta Kalaykhan-Sewradj for her administrative work. Lastly, we would like to thank all research technicians and participants for their contribution to the study.

Author contributions Conceptualization: Martin Schilder, Stefano Mandija, Alessandro Sbrizzi; Methodology: Martin Schilder; formal analysis: Martin Schilder; investigation: Stefano Mandija, Sarah Jacobs, Beyza Köktaş; software: Hanna Liu, Oscar van der Heide, Federico D'Agata; data curation: Stefano Mandija, Sarah Jacobs, Jordi Kleinloog, Vera Keil, Evert-Jan Vonken, Jan Willem Dankbaar, Jeroen Hendrikse, Tom Snijders, Anja van der Kolk; writing—original draft preparation: Martin Schilder, Stefano Mandija, Alessandro Sbrizzi; writing—review and editing: Sarah Jacobs, Jordi Kleinloog, Vera Keil, Evert-Jan Vonken, Jan Willem Dankbaar, Tom Snijders, Cornelis van den Berg, Anja van der Kolk; funding acquisition: Alessandro Sbrizzi; supervision: Jeroen Hendrikse, Cornelis van den Berg, Anja van der Kolk, Alessandro Sbrizzi.

Funding Netherlands Organisation for Scientific Research (NWO) Demonstrator Grant 16937.

Data availability Example images of the quantitative parameter maps (T_1, T_2, PD) and conventional and synthetic contrast weighted images including all 30 slices from a healthy participant and a patient of each group are in a publicly available repository (https://gitlab.com/asbrizzi/mr-stat-synthetic-images).

Declarations

Conflict of interest Not applicable.

Ethical standard This study was approved by the Institutional Ethics Review Board (NL69544.041.19, METC 19/282).

References

1. Sbrizzi A, van der Heide O, Cloos M, van der Toorn A, Hoogduin H, Luijten PR, van den Berg CAT (2018) Fast quantitative MRI as a nonlinear tomography problem. Magn Reson Imaging 46:56–63. https://doi.org/10.1016/j.mri.2017.10.015
2. Keil VC, Bakoeva SP, Jurcoane A, Doneva M, Amthor T, Koken P, Mädler B, Lüchters G, Block W, Wüllner U et al (2020) A pilot study of magnetic resonance fingerprinting in Parkinson's disease. NMR Biomed. https://doi.org/10.1002/nbm.4389

3. Schmitt P, Griswold MA, Jakob PM, Kotas M, Gulani V, Flentje M, Haase A (2004) Inversion recovery TrueFISP: quantification of T1, T2, and spin density. Magn Reson Med 51(4):661–667. https://doi.org/10.1002/mrm.20058
4. Warntjes JBM, Dahlqvist O, Lundberg P (2007) Novel method for rapid, simultaneous T1, T*2, and proton density quantification. Magn Reson Med 57(3):528–537. https://doi.org/10.1002/mrm.21165
5. Ma D, Gulani V, Seiberlich N, Liu K, Sunshine JL, Duerk JL, Griswold MA (2013) Magnetic resonance fingerprinting. Nature 495(7440):187–192. https://doi.org/10.1038/nature11971
6. Badve C, Yu A, Rogers M, Ma D, Liu Y, Schluchter M, Sunshine J, Griswold M, Gulani V (2015) Simultaneous T1 and T2 brain relaxometry in asymptomatic volunteers using magnetic resonance fingerprinting. Tomography 1(2):136–144. https://doi.org/10.18383/j.tom.2015.00166
7. Benjamin AJV, Gómez PA, Golbabaee M, Mahbub ZB, Sprenger T, Menzel MI, Davies M, Marshall I (2019) Multi-shot echo planar imaging for accelerated Cartesian MR fingerprinting: an alternative to conventional spiral MR fingerprinting. Magn Reson Imaging 61:20–32. https://doi.org/10.1016/j.mri.2019.04.014
8. Choi JY, Hu S, Su T-Y, Murakami H, Tang Y, Blümcke I, Najm I, Sakaie K, Jones S, Griswold M et al (2023) Normative quantitative relaxation atlases for characterization of cortical regions using magnetic resonance fingerprinting. Cereb Cortex 33(7):3562–3574. https://doi.org/10.1093/cercor/bhac292
9. Chen Y, Liu S, Wang Y, Kang Y, Haacke EM (2018) Strategically Acquired Gradient Echo (STAGE) imaging, part I: creating enhanced T1 contrast and standardized susceptibility weighted imaging and quantitative susceptibility mapping. Magn Reson Imaging 46:130–139. https://doi.org/10.1016/j.mri.2017.10.005
10. Haacke EM, Chen Y, Utriainen D, Wu B, Wang Y, Xia S, He N, Zhang C, Wang X, Lagana MM et al (2020) STrategically Acquired Gradient Echo (STAGE) Imaging, part III: technical advances and clinical applications of a rapid multi-contrast multi-parametric brain imaging method. Magn Reson Imaging 65:15–26. https://doi.org/10.1016/j.mri.2019.09.006
11. Wang Y, Chen Y, Wu D, Wang Y, Sethi SK, Yang G, Xie H, Xia S, Haacke EM (2018) STrategically Acquired Gradient Echo (STAGE) imaging, part II: correcting for RF inhomogeneities in estimating T1 and proton density. Magn Reson Imaging 46:140–150. https://doi.org/10.1016/j.mri.2017.10.006
12. Hagiwara A, Warntjes M, Hori M, Andica C, Nakazawa M, Kumamaru KK, Abe O, Aoki S (2017) SyMRI of the brain. Invest Radiol 52(10):647–657. https://doi.org/10.1097/RLI.0000000000000365
13. Ndengera M, Delattre BMA, Scheffler M, Lövblad K, Meling TR, Vargas MI (2022) Relaxation time of brain tissue in the elderly assessed by synthetic MRI. Brain Behav. https://doi.org/10.1002/brb3.2449
14. Ma S, Nguyen CT, Han F, Wang N, Deng Z, Binesh N, Moser FG, Christodoulou AG, Li D (2020) Three-dimensional simultaneous brain T 1, T 2, and ADC mapping with MR multitasking. Magn Reson Med 84(1):72–88. https://doi.org/10.1002/mrm.28092
15. Ma S, Wang N, Fan Z, Kaisey M, Sicotte NL, Christodoulou AG, Li D (2021) Three-dimensional whole-brain simultaneous T1, T2, and T1 ρ quantification using MR multitasking: method and initial clinical experience in tissue characterization of multiple sclerosis. Magn Reson Med 85(4):1938–1952. https://doi.org/10.1002/mrm.28553
16. Cao T, Ma S, Wang N, Gharabaghi S, Xie Y, Fan Z, Hogg E, Wu C, Han F, Tagliati M et al (2022) Three-dimensional simultaneous brain mapping of T1, T2, and magnetic susceptibility with MR multitasking. Magn Reson Med 87(3):1375–1389. https://doi.org/10.1002/mrm.29059
17. van der Heide O, Sbrizzi A, Luijten PR, van den Berg CAT (2020) High-resolution in vivo MR-STAT using a matrix-free and parallelized reconstruction algorithm. NMR Biomed 33(4):e4251. https://doi.org/10.1002/nbm.4251
18. van der Heide O, Sbrizzi A, van den Berg CAT (2020) Accelerated MR-STAT reconstructions using sparse Hessian approximations. IEEE Trans Med Imaging 39(11):3737–3748. https://doi.org/10.1109/TMI.2020.3003893
19. Mandija S, D'Agata F, Liu H, van der Heide O, Koktas B, van den Berg CAT (2020) A five-minute multi-parametric high-resolution whole-brain MR-STAT exam: first results from a clinical trial. In: Proceedings of the International Society for Magnetic Resonance in Medicine, vol 28
20. Kleinloog JPD, Mandija S, D'Agata F, Liu H, van der Heide O, Koktas B, Dankbaar JW, Keil VC, Vonken E-J, Jacobs SM et al (2023) Synthetic MRI with Magnetic Resonance Spin TomogrAphy in Time-Domain (MR-STAT): results from a prospective cross-sectional clinical trial. J Magn Reson Imaging 57(5):1451–1461. https://doi.org/10.1002/jmri.28425
21. Liu H, van der Heide O, Mandija S, van den Berg CAT, Sbrizzi A (2022) Acceleration strategies for MR-STAT: achieving high-resolution reconstructions on a desktop PC Within 3 minutes. IEEE Trans Med Imaging 41(10):2681–2692. https://doi.org/10.1109/TMI.2022.3168436
22. Liu H, van der Heide O, Versteeg E, Froeling M, Fuderer M, Xu F, van den Berg CAT, Sbrizzi A (2024) A three-dimensional magnetic resonance spin tomography in time-domain protocol for high-resolution multiparametric quantitative magnetic resonance imaging. NMR Biomed. https://doi.org/10.1002/nbm.5050
23. Liu H, Versteeg E, Fuderer M, van der Heide O, Schilder MB, van den Berg CAT, Sbrizzi A (2024) Time-efficient, high-resolution 3T whole-brain relaxometry using Cartesian 3D MR Spin TomogrAphy in Time-Domain (MR-STAT) with cerebrospinal fluid suppression. Magn Reson Med. https://doi.org/10.1002/mrm.30384
24. van der Heide O, Fuderer M, Liu H, van den Berg C, Sbrizzi A (2022) Repeatability and accuracy of MR-STAT quantitative T1 and T2 measurements. Proc Intl Soc Mag Reson Med. https://doi.org/10.58530/2022/2796
25. Okubo G, Okada T, Yamamoto A, Fushimi Y, Okada T, Murata K, Togashi K (2017) Relationship between aging and T_1 relaxation time in deep gray matter: a voxel-based analysis. J Magn Reson Imaging 46(3):724–731. https://doi.org/10.1002/jmri.25590
26. Hagiwara A, Fujimoto K, Kamagata K, Murata S, Irie R, Kaga H, Someya Y, Andica C, Fujita S, Kato S et al (2021) Age-related changes in relaxation times, proton density, myelin, and tissue volumes in adult brain analyzed by 2-dimensional quantitative synthetic magnetic resonance imaging. Invest Radiol 56(3):163–172. https://doi.org/10.1097/RLI.0000000000000720
27. Manjón JV, Romero JE, Vivo-Hernando R, Rubio G, Aparici F, de la Iglesia-Vaya M, Coupé P (2022) Vol2Brain: a new online pipeline for whole brain MRI analysis. Front Neuroinform. https://doi.org/10.3389/fninf.2022.862805
28. McCarthy P (2023) FSLeyes. https://doi.org/10.5281/ZENODO.8033457
29. Cao X, Ye H, Liao C, Li Q, He H, Zhong J (2019) Fast 3D brain MR fingerprinting based on multi-axis spiral projection trajectory. Magn Reson Med 82(1):289–301. https://doi.org/10.1002/mrm.27726
30. Khajehim M, Christen T, Tam F, Graham SJ (2021) Streamlined magnetic resonance fingerprinting: fast whole-brain coverage with deep-learning based parameter estimation. Neuroimage 238:118237. https://doi.org/10.1016/j.neuroimage.2021.118237
31. Cao X, Liao C, Iyer SS, Wang Z, Zhou Z, Dai E, Liberman G, Dong Z, Gong T, He H et al (2022) Optimized multi-axis spiral projection MR fingerprinting with subspace reconstruction for rapid whole-brain high-isotropic-resolution quantitative imaging.

Magn Reson Med 88(1):133–150. https://doi.org/10.1002/mrm.29194
32. Konar AS, Shah AD, Paudyal R, Fung M, Banerjee S, Dave A, Hatzoglou V, Shukla-Dave A (2022) Quantitative relaxometry metrics for brain metastases compared to normal tissues: a pilot MR fingerprinting study. Cancers (Basel) 14(22):5606. https://doi.org/10.3390/cancers14225606
33. Zou L, Liang D, Ye H, Su S, Zhu Y, Liu X, Zheng H, Wang H (2021) Quantitative MR relaxation using MR fingerprinting with fractional-order signal evolution. J Magn Reson 330:107042. https://doi.org/10.1016/j.jmr.2021.107042
34. Assländer J, Cloos MA, Knoll F, Sodickson DK, Hennig J, Lattanzi R (2018) Low rank alternating direction method of multipliers reconstruction for MR fingerprinting. Magn Reson Med 79(1):83–96. https://doi.org/10.1002/mrm.26639
35. Lu L, Chen Y, Shen C, Lian J, Das S, Marks L, Lin W, Zhu T (2020) Initial assessment of 3D magnetic resonance fingerprinting (MRF) towards quantitative brain imaging for radiation therapy. Med Phys 47(3):1199–1214. https://doi.org/10.1002/mp.13967
36. Chen Y, Fang Z, Hung S-C, Chang W-T, Shen D, Lin W (2020) High-resolution 3D MR fingerprinting using parallel imaging and deep learning. Neuroimage 206:116329. https://doi.org/10.1016/j.neuroimage.2019.116329
37. Cao P, Cui D, Vardhanabhuti V, Hui ES (2020) Development of fast deep learning quantification for magnetic resonance fingerprinting in vivo. Magn Reson Imaging 70:81–90. https://doi.org/10.1016/j.mri.2020.03.009
38. Rieger B, Akçakaya M, Pariente JC, Llufriu S, Martinez-Heras E, Weingärtner S, Schad LR (2018) Time efficient whole-brain coverage with MR fingerprinting using slice-interleaved echo-planar-imaging. Sci Rep 8(1):6667. https://doi.org/10.1038/s41598-018-24920-z
39. Nagtegaal M, Koken P, Amthor T, Doneva M (2020) Fast multi-component analysis using a joint sparsity constraint for MR fingerprinting. Magn Reson Med 83(2):521–534. https://doi.org/10.1002/mrm.27947
40. Deshmane A, McGivney DF, Ma D, Jiang Y, Badve C, Gulani V, Seiberlich N, Griswold MA (2019) Partial volume mapping using magnetic resonance fingerprinting. NMR Biomed 32(5):e4082. https://doi.org/10.1002/nbm.4082
41. Körzdörfer G, Kirsch R, Liu K, Pfeuffer J, Hensel B, Jiang Y, Ma D, Gratz M, Bär P, Bogner W et al (2019) Reproducibility and repeatability of MR fingerprinting relaxometry in the human brain. Radiology 292(2):429–437. https://doi.org/10.1148/radiol.2019182360
42. Buonincontri G, Biagi L, Retico A, Cecchi P, Cosottini M, Gallagher FA, Gómez PA, Graves MJ, McLean MA, Riemer F et al (2019) Multi-site repeatability and reproducibility of MR fingerprinting of the healthy brain at 1.5 and 3.0 T. Neuroimage 195:362–372. https://doi.org/10.1016/j.neuroimage.2019.03.047
43. Ma D, Jones SE, Deshmane A, Sakaie K, Pierre EY, Larvie M, McGivney D, Blümcke I, Krishnan B, Lowe M et al (2019) Development of high-resolution 3D MR fingerprinting for detection and characterization of epileptic lesions. J Magn Reson Imaging 49(5):1333–1346. https://doi.org/10.1002/jmri.26319
44. Fang Z, Chen Y, Hung S, Zhang X, Lin W, Shen D (2020) Submillimeter MR fingerprinting using deep learning-based tissue quantification. Magn Reson Med 84(2):579–591. https://doi.org/10.1002/mrm.28136
45. Hilbert T, Xia D, Block KT, Yu Z, Lattanzi R, Sodickson DK, Kober T, Cloos MA (2020) Magnetization transfer in magnetic resonance fingerprinting. Magn Reson Med 84(1):128–141. https://doi.org/10.1002/mrm.28096
46. van der Heide O, Sbrizzi A, van den Berg CAT (2023) Cartesian vs radial MR-STAT: an efficiency and robustness study. Magn Reson Imaging 99:7–19. https://doi.org/10.1016/j.mri.2023.01.017
47. Sun T, Walsh CA (2006) Molecular approaches to brain asymmetry and handedness. Nat Rev Neurosci 7(8):655–662. https://doi.org/10.1038/nrn1930
48. Springer E, Cardoso PL, Strasser B, Bogner W, Preusser M, Widhalm G, Nittka M, Koerzdoerfer G, Szomolanyi P, Hangel G et al (2022) MR Fingerprinting—a radiogenomic marker for diffuse gliomas. Cancers (Basel) 14(3):723. https://doi.org/10.3390/cancers14030723
49. Filippi M, Rocca MA, Ciccarelli O, De Stefano N, Evangelou N, Kappos L, Rovira A, Sastre-Garriga J, Tintorè M, Frederiksen JL et al (2016) MRI criteria for the diagnosis of multiple sclerosis: MAGNIMS Consensus guidelines. Lancet Neurol 15(3):292–303. https://doi.org/10.1016/S1474-4422(15)00393-2
50. Blystad I, Håkansson I, Tisell A, Ernerudh J, Smedby Ö, Lundberg P, Larsson E-M (2016) Quantitative MRI for analysis of active multiple sclerosis lesions without gadolinium-based contrast agent. Am J Neuroradiol 37(1):94–100. https://doi.org/10.3174/ajnr.A4501
51. Bonnier G, Roche A, Romascano D, Simioni S, Meskaldji D, Rotzinger D, Lin Y, Menegaz G, Schluep M, Du Pasquier R et al (2014) Advanced MRI unravels the nature of tissue alterations in early multiple sclerosis. Ann Clin Transl Neurol 1(6):423–432. https://doi.org/10.1002/acn3.68
52. Holland MA, Budday S, Li G, Shen D, Goriely A, Kuhl E (2020) Folding drives cortical thickness variations. Eur Phys J Spec Top 229(17–18):2757–2778. https://doi.org/10.1140/epjst/e2020-000001-6
53. Feraco P, Gagliardo C, La Tona G, Bruno E, D'angelo C, Marrale M, Del Poggio A, Malaguti MC, Geraci L, Baschi R et al (2021) Imaging of substantia Nigra in Parkinson's disease: a narrative review. Brain Sci 11(6):769. https://doi.org/10.3390/brainsci11060769
54. Piredda GF, Hilbert T, Granziera C, Bonnier G, Meuli R, Molinari F, Thiran J, Kober T (2020) Quantitative brain relaxation atlases for personalized detection and characterization of brain pathology. Magn Reson Med 83(1):337–351. https://doi.org/10.1002/mrm.27927